Journal of Computer Assisted Tomography
22(6):945–952

Activation Patterns of Covert Word Generation Detected by fMRI: Comparison with 3D PET

Norihiro Sadato, Yoshiharu Yonekura, Hiroki Yamada, Satoshi Nakamura, Atsuo Waki, and Yasushi Ishii

Purpose: The aim of our study was to compare the activation patterns of higher cognitive function detected by functional MRI (fMRI) with those by $H_2{}^{15}O$ positron emission tomography (PET).

Method: Activation studies with both modalities were performed in six normal volunteers with identical covert word generation tasks and statistical analysis. For PET, each subject had five rest scans and five task scans at 10 min intervals. fMRI was performed with a 1.5 T magnet using T2*-weighted echo planar sequences. Each scanning session consisted of two rest and two task periods of 30 s each, alternating rest and task.

Results: In group analysis, the activation patterns on both PET and fMRI were similar, whereas the deactivation patterns differed, presumably due to the noise of fMRI. In single-subject analysis, PET showed fewer activated areas and fMRI showed more areas of activation than in group analysis.

Conclusion: fMRI has an advantage over 3D PET in its better signal-to-noise ratio for detecting change in neuronal activity for higher brain function.

Index Terms: Magnetic resonance imaging, functional (fMRI)—Emission computed tomography—Image registration—Brain, metabolism.

Advances in MRI have made it possible to study activation of the human brain with whole-brain coverage using echo planar imaging and the blood oxygen level-dependent (BOLD) technique (1,2). Functional MRI (fMRI) can detect the signal change influenced by changes in regional cerebral blood flow (rCBF) through hemoglobin/deoxyhemoglobin imbalance or an inflow effect. The advantages of fMRI are better spatial and temporal resolution, widely available hardware, and no radiation exposure. In addition, whole-brain coverage enables the registration of each volume, which is essential to eliminate false ''activation'' due to task-related head motion, and it depicts discrete neuronal networks over the whole brain. In the last decade, activation studies have been based mainly on positron emission tomography (PET). Because of the known relationship between neuronal activity and CBF changes (3) and well established quantification (4,5) and statistical (6–11) methods, PET is purported to be the gold standard for activation studies. Despite this claim, direct comparisons between PET and fMRI with higher cognitive tasks are few. Direct comparison of fMRI and PET has been attempted (12), but only with partial coverage of the primary motor area due mainly to hardware limitation. fMRI with whole-brain coverage has been reported (13,14), without comparison with PET. Recently, Kim et al. (15) compared functional activation by BOLD- and CBF-based fMRI with PET during sequential finger movements, focusing mainly on the primary motor area. To evaluate fMRI in its activation pattern of higher brain function, which may activate association cortex, we directly compared fMRI with 3D PET with $H_2{}^{15}O$, using the same covert word generation task, in the identical subjects, and using the same statistical analysis.

MATERIALS AND METHODS

We studied six normal volunteers, all men, 24–33 years old (mean 26.6 years). The subjects were all right-handed by the Edinburgh Handedness Inventory (16). The protocol was approved by the ethical committee of

From the Biomedical Imaging Research Center (N. Sadato, Y. Yonekura, S. Nakamura, A. Waki, and Y. Ishii) and Department of Radiology (H. Yamada and Y. Ishii), Fukui Medical University, 23 Shimoaizuki, Matsuoka, Yoshida, Fukui, 910-11, Japan. Address correspondence and reprint requests to Dr. N. Sadato.

Fukui Medical University, and all subjects gave their written informed consent for the study.

In a verbal fluency task (17–19), subjects were given a word and required to generate as many words as they could without overtly pronouncing the words. The priming words, which were selected from standardized pictures of Songrass and Vanderwart (20), were verbally given every 6 s. Subjects underwent training sessions 2 days before the PET scan. Their performance of word generation was measured just before and after the PET scans, having them overtly pronounce verbs and nouns in response to priming words that were different from those used in the training or scanning sessions. All six subjects generated 1.9–3.7 words in 6 s.

PET

A small plastic catheter was placed in the left cubital vein for injection of the radioisotope. The subject lay in a supine position with the eyes covered. The subject's head was immobilized with an elastic band and sponge cushions. Each subject had 10 consecutive scans (five rest scans and five task scans) performed at 10 min intervals. For the rest scans, the subject lay quietly and was asked to avoid thinking of words. The first three task conditions were for verb generation, and the other two were for noun generation. Twenty seconds before $H_2{}^{15}O$ injection, the subject was verbally given a priming word and commenced word generation. Every 6 s, a different priming word was given until the end of the scan. A total of 20 words was given in each scanning session. The rest and task conditions were alternated; three subjects started with the rest condition, and the others started with the task condition.

PET scanning was performed with a GE Advance tomograph (GE, Milwaukee, WI, U.S.A.) with the interslice septa retracted. The performance characteristics of this scanner have been described in detail by DeGrado et al. (21) and Lewellen et al. (22). The scanner acquires 35 slices with interslice spacing of 4.25 mm. In the 3D mode, the scanner acquires oblique sinograms with a maximum cross-coincidence of ±11 rings. A 10 min transmission scan using two rotating ^{68}Ge sources was performed for attenuation correction. Images of CBF were obtained by summing the activity during the 60 s period following the first detection of an increase in cerebral radioactivity after the intravenous bolus injection of 10 mCi of ^{15}O-labeled water (23). The images were reconstructed with the Kinahan-Rogers reconstruction algorithm (24). Hanning filters were used, giving transaxial and axial resolutions of 6 and 10 mm full-width at half-maximum, respectively. The field of view (FOV) and pixel size of the reconstructed images were 256 and 2 mm, respectively. No arterial blood sampling was performed, and thus the images collected were those of tissue activity. Tissue activity recorded by this method is near-linearly related to rCBF (4,5).

fMRI

fMRI studies followed PET within 2 weeks. Each subject had four scans: two for verb generation and two for noun generation. Throughout the scan, the subject's eyes were closed. Each scanning session consisted of two rest and two task periods; each period was 30 s long, alternating rest and task. An on-off cycle of 60 s (30 s rest and 30 s task) was chosen to maximize the induced signal amplitude and to obtain a stable plateau of signal enhancement induced by the task (25). During rest periods, no task was required. During task periods, a priming word was given verbally through a speaker every 6 s. Subjects were instructed to generate as many verbs or nouns as possible. The priming words were different from those used in the training session or PET scan.

A time course series of 43 volumes were acquired using T2*-weighted, gradient echo, echo planar sequences with a 1.5 T GE Horizon MR imager. Each volume consisted of 11 slices, and the slice thickness was 8 mm, with a 1 mm gap, to cover the entire cerebral cortex. The time interval between two successive acquisitions of the same image was 3,000 ms and TE was 40 ms. The FOV was 24 cm. The digital in-plane resolution was 64 × 64 pixels with a pixel dimension of 3.75 × 3.75 mm. The magnetic shim was optimized such that a true in-plane resolution of 3.75 × 3.75 mm could be realized. Head motion was minimized by placing tight but comfortable foam padding around the subject's head.

Data Analysis

The data were analyzed with statistical parametric mapping (using software from the Wellcome Department of Cognitive Neurology, London, U.K.) and implemented in Matlab (Mathworks, Sherborn, MA, U.S.A.) (6–11).

The PET scans from each subject were realigned using the first image as a reference. Following realignment, all images were transformed into a standard stereotaxic space (26) using PET data. The parameters for affine and quadratic transformation to a template that was already fit for Talairach space were estimated by least-squares means (10). To determine if there was any significant difference in the activation patterns due to nonlinear transformation, anatomical normalization with only linear transformation was also performed.

Both group and single-subject statistical analyses were performed on the anatomically normalized data. In group analysis, after specifying the appropriate design matrix, the condition and subject effects were estimated according to the general linear model at each and every voxel (11). The effect of global CBF fluctuation was eliminated by using either analysis of covariance (ANCOVA) (7) or proportional scaling (global normalization) to detect any differences in the activation patterns yielded by the two methods. In single-subject analysis, global normalization was performed with proportional scaling. To test hypotheses about regionally specific condition ef-

fects, the estimates were compared by means of linear contrasts. The resulting set of voxel values for each contrast constituted a statistical parametric map of the t statistic (SPM{t}). The SPM{t} was transformed to the unit normal distribution (SPM{Z}). The threshold for SPM{Z} was set at $Z > 2.8$ and $p < 0.05$ with a correction for multiple comparisons to keep the false-positive rate at the defined level ($p < 0.05$ at either cluster level or voxel level) for the entire brain (9,11).

The first three volumes of each fMRI scan were discarded because of nonsteady condition of magnetization, and the remaining 40 volumes were used for analysis. Following realignment, all images were transformed into a standard stereotaxic space (26) using fMRI data. With use of a least-squares algorithm to evaluate the parameters for affine transformation, the experimental images were matched with the standard T2-weighted image template, previously mapped onto Talairach space (10).

Both group and single-subject statistical analyses were performed on the anatomically normalized data. In group analysis, after specifying the appropriate design matrix, delayed box-car function as a reference waveform, the condition, slow hemodynamic fluctuation unrelated to the tasks, and subject effects were estimated according to the general linear model at each and every voxel, taking spatial and temporal smoothness into account (9,11). Global normalization was performed using proportional scaling. To test hypotheses about regionally specific condition effects, the estimates were compared by means of linear contrasts of each rest and task period. The generation of SPM{Z} was identical to that of PET, with the same statistical threshold.

RESULTS

PET Group Analysis

Group analysis showed activation of the supplementary motor area (SMA), anterior cingulate gyrus, left premotor area, left Broca area, left dorsolateral prefrontal cortex, left posterior temporal region extending to the left inferior parietal lobule, and right posterior temporal region during covert word generation (Fig. 1) (Table 1). The size, location, and maximal statistical significance of activated clusters were similar among different combinations of anatomical normalization (linear + nonlinear vs. linear only) and global normalization (proportional scaling vs. ANCOVA) (Table 2). There was no significant difference in activation between verb generation and noun generation by direct comparison.

A significant decrease in rCBF was found in the medial frontal lobes, right inferior parietal lobule extending to the temporal operculum, precuneus/cuneus region, left temporal tip, and right primary sensorimotor cortex (SM1). The deactivation pattern was similar among different combinations of anatomical normalization (linear + nonlinear vs. linear only) and global normalization (Fig. 2) (Table 2).

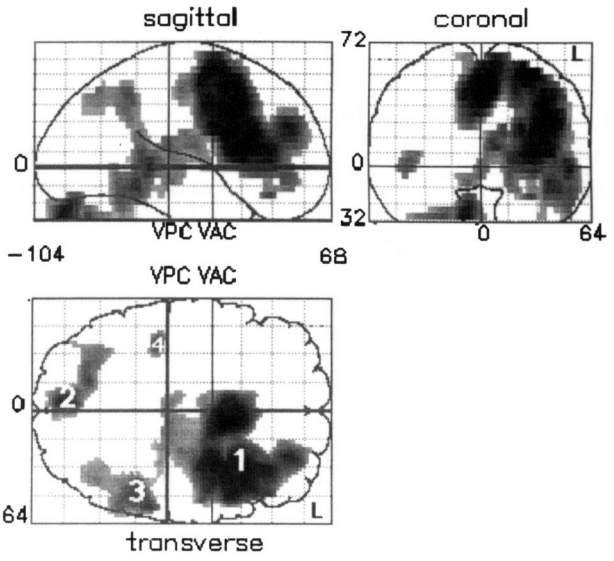

FIG. 1. Group analysis of PET activation during covert word generation compared with rest condition. Three orthogonal "line-of-sight" projections are presented. Pixels that survived the threshold of $Z > 2.8$ and $p < 0.05$ with correction for multiple comparisons are shown. The number on each discrete focus of activation corresponds to the location shown in Table 2.

fMRI Group Analysis

The activation pattern on fMRI was similar to that on PET (Fig. 3). Covert word generation activated the SMA, anterior cingulate gyrus, left premotor area, left Broca area, left dorsal prefrontal cortex, left posterior temporal region, thalamus bilaterally, and basal ganglia. The extent of cerebellar activation was on fMRI somewhat smaller in its extent than on PET, probably due to the limited axial FOV. No significant difference was noted between verb generation and noun generation.

The deactivation (negative activation) pattern on fMRI was different from that on PET (Fig. 4). During word generation, deactivation was observed in the right medial prefrontal region and the occipital cortex, including the precuneus/cuneus region extending to the right ventral occipital region (Fig. 4).

Single-Subject Analysis

Compared with the results of group analysis, single-subject analysis of PET data detected smaller and fewer activated areas (Fig. 5). Single-subject analysis of fMRI data showed activation comparable with that revealed by group analysis (Fig. 6). However, several activated foci did not fit within the template margins (Fig. 6). Deactivation showed the same tendency.

DISCUSSION

Procedures of Data Analysis

To evaluate whether fMRI was superior to $H_2{}^{15}O$ PET in detecting changes in neuronal activity of the human

TABLE 1. *Covert word generation by PET (with linear transformation and proportional scaling)*

Cluster size	Cluster (Pat cluster-level)	Activation Talairach's Coordinates x	y	z	Z(**)	Location(*)
5965	0.000	−4	8	44	48.64 (<0.01)	lt ACG(32)
		−28	−2	56	7.53 (<0.01)	lt PMd(6)
		−40	10	28	7.47 (<0.01)	lt GFi(44)
367	0.072	8	−86	−28	6.50 (<0.01)	rt cerebell
1048	0.002	−52	−38	0	5.77 (<0.01)	lt GTm(21)
70	0.523	40	−34	0	4.41 (0.017)	rt GTm(21)
		Deactivation				
3275	0.000	50	−28	24	6.70 (<0.01)	rt LPi(40)
		50	−56	16	5.84 (<0.01)	rt GTs(22)
		40	18	−16	7.47 (<0.01)	rt GTs(38)
2373	0.000	12	58	8	6.66 (<0.01)	rt GFd(10)
		24	28	40	5.69 (<0.01)	rt GFm(8)
1085	0.002	10	−66	32	5.64 (<0.01)	rt PCu(7)
		2	−66	20	5.23 (<0.01)	rt PCu(31)
135	0.328	−8	−16	36	4.97 (<0.01)	lt GC(24)
114	0.381	−50	4	−20	4.87 (<0.01)	lt GTm(21)
54	0.588	22	−22	60	4.57 (<0.01)	rt SM1

* Brodmann area according to Talairach and Tournoux (26).

ACG, anterior cingulate gyrus; GC, cingulate gyrus; GFd, medial frontal gyrus; GFi, inferior frontal gyrus; GFm, middle frontal gyrus; GTm, middle temporal gyrus; GTs, superior temporal gyrus; LPi, inferior parietal lobule; PCu, precuneus; PMd, dorsal premotor cortex; SM1, primary sensorimotor cortex.

** P value at voxel level with correction for multiple comparisons.

brain, we compared the overall differences of the modalities by group analysis in addition to single-subject analysis. To ensure that the results of the fMRI and PET analyses were comparable, several procedures not frequently applied to fMRI or PET were performed.

TABLE 2. *Effect of anatomical and global normalization on size and significance of activated areas by PET. P values at cluster-level (size, height) with threshold of Z > 2.8 are shown.*

Global normalization	Location	Activation Anatomical normalization: Linear + 3D nonlinear	Linear
Proportional	1	0.000 (5940, 8.55)	0.000 (5965, 8.64)
	2	0.025 (403, 6.54)	0.033 (367, 6.50)
	3	0.000 (1016, 5.64)	0.000 (1048, 5.77)
	4	0.589 (62, 4.37)	0.542 (70, 4.41)
ANCOVA	1	0.000 (5255, 7.72)	0.000 (5318, 7.88)
	2	0.051 (306, 6.08)	0.061 (286, 0.061)
	3	0.000 (943, 5.68)	0.000 (968, 5.60)
	4	0.533 (72, 4.75)	0.488 (80, 0.488)
		Deactivation	
Proportional	1	0.000 (2260, 6.72)	0.000 (2373, 6.66)
	2	0.000 (3173, 6.37)	0.000 (3275, 6.70)
	3	0.000 (1119, 5.46)	0.000 (1085, 5.64)
	4	0.242 (152, 5.14)	0.283 (135, 4.97)
	5	0.390 (104, 4.73)	0.349 (114, 4.87)
	6	0.708 (42, 4.29)	0.632 (54, 4.57)
ANCOVA	1	0.000 (2083, 6.65)	0.000 (2145, 6.55)
	2	0.000 (2634, 5.72)	0.000 (2546, 5.76)
	3	0.001 (813, 4.94)	0.001 (758, 5.04)
	4	0.348 (113, 4.75)	0.459 (86, 4.56)
	5	0.294 (129, 4.62)	0.331 (117, 4.92)

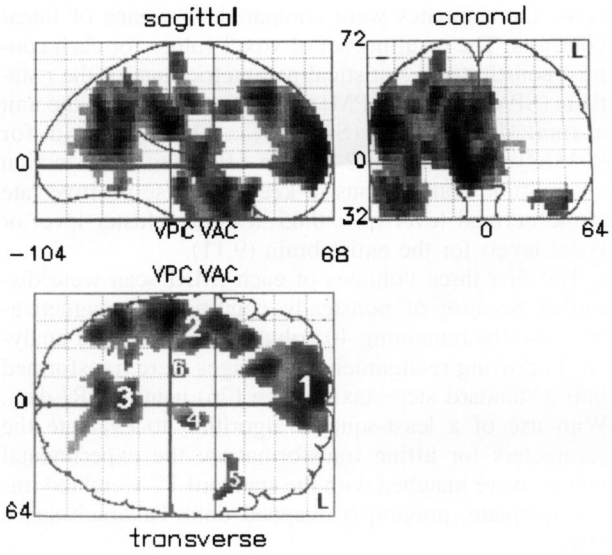

FIG. 2. Group analysis of PET deactivation during covert word generation compared with rest condition. Details are the same as for Fig. 1.

Anatomical normalization is essential for group analysis of PET, whereas fMRI does not necessarily require this procedure because single-subject data of fMRI usually provide enough statistical power. Anatomical nor-

TABLE 3. *Covert word generation by fMRI*

Size	Cluster (Pat cluster-level)	Activation Talairach's coordinates x	y	z	Z(**)	Location(*)
3057	<0.001	0	2	52	8.87 (<0.01)	SMA
		−46	26	20	8.57 (<0.01)	lt GFi(45)
		−46	−2	36	7.47 (<0.01)	lt GPrC(6)
2726	<0.001	−20	−16	4	7.88 (<0.01)	lt Thalamus
		−18	−4	−8	5.04 (<0.01)	lt Amygdala
		−4	−18	8	7.22 (<0.01)	lt Thalamus
239	<0.001	−58	−52	−12	6.56 (<0.01)	lt GTi(37)
		−52	−48	−16	6.28 (<0.01)	lt GF(37)
		−62	−28	−4	4.38 (0.046)	lt GTm(21)
121	0.234	−32	−78	36	4.68 (0.014)	lt GOs(19)
68	0.504	−10	−102	−12	4.97 (0.004)	lt GL(17)
		Deactivation				
4833	<0.001	0	−84	24	8.37 (<0.01)	Cu(18)
		2	−80	36	8.08 (<0.01)	rt Cu(19)
		−4	−58	36	7.77 (<0.01)	lt PCu(7)
1403	<0.001	24	34	40	8.01 (<0.01)	rt GFm(8)
		4	60	8	7.84 (<0.01)	rt GFd(10)
		14	54	28	7.80 (<0.01)	rt GFs(9)
193	0.084	−40	−86	−8	5.65 (<0.01)	lt GOi(18)
13	0.939	52	8	12	4.63 (0.016)	rt GFi(44)

* Brodmann Area according to Talairach and Tournoux (26).

Cu, cuneus; GF, fusiform gyrus; GFi, inferior frontal gyrus; GFd, medial frontal gyrus; GFi, inferior frontal gyrus; GFm, middle frontal gyrus; GFs, superior frontal gyrus; GL, lingual gyrus; GOi, inferior occipital gyrus; GOs, superior occipital gyrus; GPrC, precentral gyrus; GTi, inferior temporal gyrus; GTm, middle temporal gyrus; GTs, superior temporal gyrus; LPi, inferior parietal lobule; PCu, precuneus; SMA, supplementary motor area.

** P value at voxel level with correction for multiple comparisons.

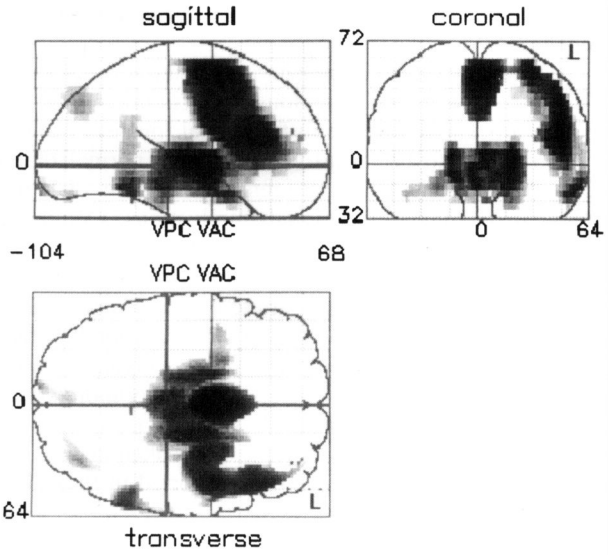

FIG. 3. Group analysis of fMRI activation during covert word generation compared with the rest condition. Pixels that survived the threshold of $Z > 2.8$ and $p < 0.05$ with correction for multiple comparisons are shown.

malization has been developed for standardization of PET data to eliminate the anatomical variability among subjects, primarily to increase the signal-to-noise ratio, as PET data from single subjects are usually limited in terms of degrees of freedom for determining statistical inference. Although nonlinear transformation is frequently used in PET data analysis to decrease anatomical variance, a linearly transformed PET data set gave equivalent activation with this particular task (Table 2). Hence, we compared linearly transformed data of PET and fMRI.

Global Normalization

The relationship between global CBF and rCBF has been extensively discussed in the PET literature (5,7). Without global normalization, regional changes of CBF or local neuronal activation cannot be properly detected. It has been shown that ANCOVA and proportional scaling give essentially the same results (7). However, in fMRI, a signal change indirectly reflects a change in rCBF (1), although the signal itself is determined by various factors other than flow. Hence, proportional scaling applied to fMRI data in this study was to eliminate global fluctuation of the signal, which is not necessarily determined by global CBF change.

Time Autocorrelation

Because of relatively slow hemodynamic responses (~5 s in delay constant), consecutive fMRI scans at short intervals (3 s) have autocorrelation of the signal intensity in each pixel along the time axis. In fMRI statistical analysis, this has been estimated as decreased effective degrees of freedom (11). In PET, the scans were all 10 min apart and therefore were regarded as independent of each other.

Differences in Task-Related Activation or Deactivation

We used a word generation paradigm that has been used in many other activation studies (17–19,27,28), and its activation pattern, including the association cortex, is well recognized. This is a frequently used activation paradigm testing verbal fluency, which involves the retrieval of words from memory in response to a stimulus such as a letter prompt, a word prompt, or a superordinate category prompt (18). A number of functional imaging studies of word retrieval have been reported (27–30), agreeing about left frontal activation and the left temporal lobe involvement (18). The reproducibility of the covert word generation task identical to the present study was evaluated in a multicenter European experiment (19). Consistent activation among different institutes was observed in the left middle temporal gyrus, left superior temporal sulcus, the left inferior frontal gyrus, the middle frontal gyrus, the insula on the left, and the cerebellum on the right (19). Furthermore, Poline et al. (19) have observed that the 3D PET scanner was more sensitive than the 2D scanner in depicting activation. The expected activation pattern and its spatial extent were obtained by both PET and fMRI. The activation pattern in the cerebral cortex on both PET and fMRI was consistent with the previous findings (18,19,28). Activation in the subcortical regions, such as the thalamus and basal ganglia, which has been reported for PET (18), was more prominent on fMRI than PET. Smaller activation in the cerebellum on fMRI was due mainly to limitation of the

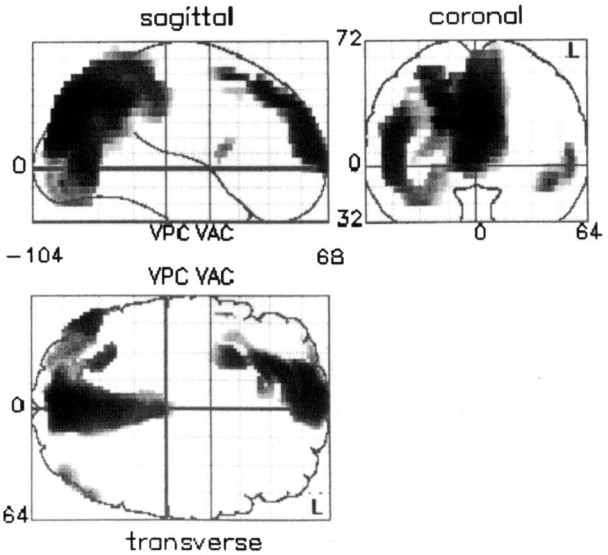

FIG. 4. Group analysis of fMRI deactivation during covert word generation compared with the rest condition. Details are the same as for Fig. 3.

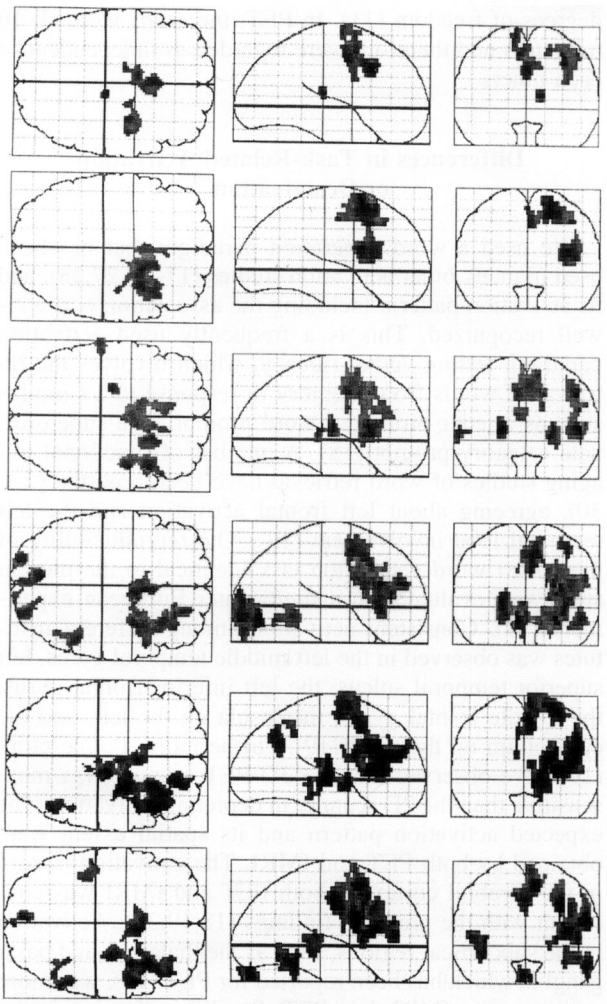

FIG. 5. Single-subject analysis of PET activation during covert generation compared with the rest condition. Raw data for all six subjects are shown. "Line-of-sight" projection views, with the same format as in Fig. 1, are shown in axial (**left**), sagittal (**middle**), and coronal (**right**) views. Pixels that survived the threshold of $Z > 2.8$ and $p < 0.05$ with correction for multiple comparisons are shown.

axial FOV (10 cm) of the particular MR scanner used in this study compared with 15 cm in PET. Higher Z score in fMRI than in PET in group analysis is due to a larger degree of freedom even after correction for autocorrelation in time series (11). In single-subject analysis, there was more underestimation of activated areas in PET than in fMRI. This was due mainly to a larger degree of freedom of fMRI. The effective degrees of freedom of single-subject fMRI was 56, whereas that of PET was 8. A small sample size has been shown to cause more false negatives, particularly with pixel-by-pixel estimation of error variance (28). The degree of freedom of fMRI was probably large enough to depict the neuronal substrates of the covert word generation in single-subject analysis, whereas PET obtained benefit from group analysis by increased degree of freedom. fMRI has an advantage over 3D PET in that its signal-to-noise ratio is better for detecting change in neuronal activity during covert word generation.

The deactivation (or negative activation) pattern of PET is consistent with previous PET findings (18). Although a negative change in functional images is sometimes thought to be an artifact of global normalization (28), the consistent and discrete localization of a decrease in rCBF has functional implications. Compared with PET, fMRI showed extensive deactivation in the occipital pole, extending to the right fusiform gyrus, but no deactivation in the right parietotemporal region. This discrepancy could be explained by the confounding factor of MR noise. As priming words were given verbally, in the noisy MR gantry, subjects had to pay more attention to the auditory modality, resulting in cross-modal depression of the visual cortex. This phenomenon of cross-modal suppression has been reported in PET activation studies (31,32).

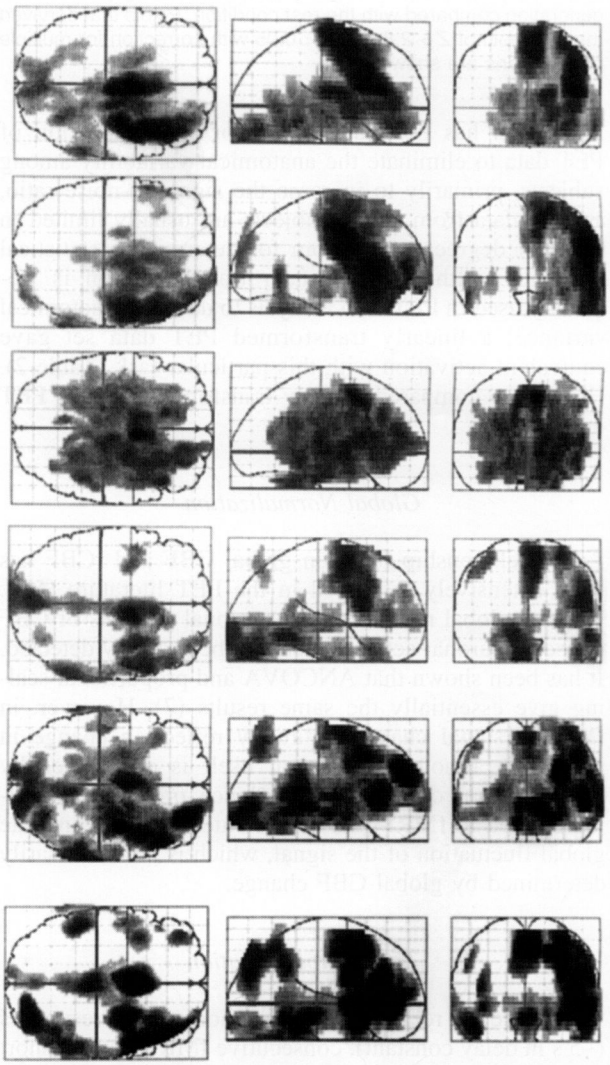

FIG. 6. Single-subject analysis of fMRI activation during covert generation compared with the rest condition. Details are the same as for Fig. 5.

Confounding Factors of fMRI

The results of fMRI should be interpreted with the following potentially confounding factors in mind: altered oxygen metabolism, interval between tasks, and image distortion due to the magnetic susceptibility effect.

Whereas the PET signal is proportional to rCBF, the signal change of fMRI is derived from changes in oxygenation of hemoglobin, which is indirectly influenced by local changes in rCBF. Therefore, differences in oxygen metabolism may affect the fMRI results. Recently, a negative signal change in the primary visual cortex during photic stimulation in infancy has been reported (33). The inverse signal response in infants has been postulated to be related to higher synaptic density and higher metabolic rate. Abnormal signal behavior might occur when an fMRI activation study is applied to subjects with altered oxygen metabolism.

Different task intervals in PET and fMRI may cause discrepancies of activation or deactivation patterns. PET is usually performed with at least 10 min intervals between each task condition; hence, it is reasonable to assume that the effect of the previous session is negligible in the subsequent session. In fMRI, however, data from each task condition are collected consecutively, alternating in 30 s. Relatively slow changes of neuronal activity elicited during one task condition could extend to the following condition (usually a rest condition) and hence might be missed by an approach with assumed reference function (25).

The magnetic susceptibility of air-containing structures in the human head produces the susceptibility artifacts. The most prominent is the signal loss due to the local field gradient in the slice selection direction (34,35). The source of the gradient echo signal loss is the strong local magnetic field gradients around the air and tissue interfaces (36). Although compensation for susceptibility inhomogeneity has been proposed (34,36), further investigation is necessary for evaluation near the base of the skull by fMRI.

Distortion of the images due to a magnetic susceptibility effect also influences anatomical transformation of fMRI into standardized Talairach space. In the present study, linear transformation was used to transform fMRI data into standardized Talairach space. Image distortion and localized signal loss of fMRI data make nonlinear transformation difficult. As PET did not show a significant difference in the final result of activation or deactivation patterns between linear and nonlinear transformation, probably the use of linear transformation in fMRI is also justified for group analysis. Although we used functional images for anatomical normalization, an alternative method would be estimation of parameters for nonlinear transformation using co-registered (or obtained in the identical locations) anatomical MRI, which does not have any image distortion, the parameters of which are applied to the fMRI data. This procedure would allow use of the smallest possible smoothing kernel for averaging over subjects; thus, better spatial resolution of fMRI would allow more accurate anatomical localization of the activated foci than PET.

Study Limitations

In the present study, all fMRI was performed after the PET scans; hence, an order effect or learning effect cannot be ruled out. However, as pre-PET training saturated the performance, any learning effect may be small. The lack of measurement of performance during the scans, due to the characteristics of the task, is another limitation because the performance during PET and fMRI may not be equivalent. However, covert word generation has been widely used in imaging studies and in particular was validated to show robust activation in a multicenter study (19). Thus, our approach may be justified as far as the methodology is concerned.

Despite these limitations, the present study showed that PET and fMRI yielded comparable activations with the same task by the identical subjects, consolidating the validity of fMRI for detecting changes in neuronal activity during higher cognitive function.

Acknowledgment: This study was supported in part by a research grant (JSPS-RFTF97L00203) from the Research for the Future Program from the Japan Society for the Promotion of Science.

REFERENCES

1. Ogawa S, Tank DW, Menon R, et al. Intrinsic signal changes accompanying sensory stimulation: functional brain mapping with magnetic resonance imaging. *Proc Natl Acad Sci USA* 1992;89: 5951–5.
2. Kwong KK, Belliveau JW, Chesler DA, et al. Dynamic magnetic resonance imaging of human brain activity during primary sensory stimulation. *Proc Natl Acad Sci USA* 1992;89:5675–9.
3. Raichle ME. Circulatory and metabolic correlates of brain function in normal humans. In: Mountcastle VB, Plum F, Geiger SR, eds. *Higher functions of the brain.* Bethesda: American Physiology Society, 1987:643–74. (Handbook of physiology, vol 5; The nervous system, sect 1).
4. Fox PT, Mintun MA. Noninvasive functional brain mapping by change-distribution analysis of averaged PET images of $H_2{}^{15}O$ tissue activity. *J Nucl Med* 1989;30:141–9.
5. Fox PT, Mintun MA, Raichle ME, Herscovitch P. A noninvasive approach to quantitative functional brain mapping with $H_2{}^{15}O$ and positron emission tomography. *J Cereb Blood Flow Metab* 1984; 4:329–33.
6. Friston KJ, Passingham RE, Nutt JG, Heather JD, Sawle GV, Fackowiak RSJ. Localisation in PET images: direct fitting of the intercommissural (AC-PC) line. *J Cereb Blood Flow Metab* 1989; 9:690–5.
7. Friston KJ, Frith CD, Liddle PF, Dolan RJ, Lammertsma AA, Frackowiak RSJ. The relationship between global and local changes in PET scans. *J Cereb Blood Flow Metab* 1990;10:458–66.
8. Friston KJ, Frith CD, Liddle PF, Frackowiak RSJ. Comparing functional (PET) images: the assessment of significant change. *J Cereb Blood Flow Metab* 1991;11:690–9.
9. Friston KJ, Worsley KJ, Frackowiak RSJ, Mazziotta JC, Evans AC. Assessing the significance of focal activations using their spatial extent. *Hum Brain Map* 1994;1:210–20.
10. Friston KJ, Ashburner J, Frith CD, Heather JD, Frackowiak RSJ.

Spatial registration and normalization of images. *Hum Brain Map* 1995;2:165–89.
11. Friston KJ, Holmes AP, Worsley KJ, Poline JB, Frith CD, Frackowiak RSJ. Statistical parametric maps in functional imaging: a general linear approach. *Hum Brain Map* 1995;2:189–210.
12. Sadato N, Ibanez V, Campbell G, Deiber M-P, Le Bihan D, Hallett M. Frequency dependent changes of regional cerebral blood flow during finger movements: functional MRI compared with PET. *J Cereb Blood Flow Metab* 1997;17:670–9.
13. Mattay VS, Frank JA, Santha AKS, et al. Whole-brain functional mapping with isotropic MR imaging. *Radiology* 1996;201:399–404.
14. Binder JR, Frost JA, Hammeke TA, Cox RW, Rao SM, Prieto T. Human brain language areas identified by functional magnetic resonance imaging. *J Neurosci* 1997;17:353–62.
15. Kim S-G, Strother SC, Sidtis J-J, et al. Comparison of functional activation studied by BOLD- and CBF-based fMRI and PET during sequential finger opposition. Proceedings of the International Society for Magnetic Resonance in Medicine 5th scientific meeting and exhibition, Vancouver, BC, Canada, 1997:379.
16. Oldfield RC. The assessment and analysis of handedness: the Edinburgh Inventory. *Neuropsychologia* 1971;9:97–113.
17. Rueckert L, Appollonio I, Grafman J, et al. Magnetic resonance imaging functional activation of left frontal cortex during covert word production. *J Neuroimag* 1994;4:67–70.
18. Warburton E, Wise RJS, Price CJ, et al. Noun and verb retrieval by normal subjects studied with PET. *Brain* 1996;119:159–79.
19. Poline J-B, Vandenberghe R, Holmes AP, Friston KJ, Frackowiak RSJ. Reproducibility of PET activation studies: lessons from a multi-center European experiment EU concerted action on functional imaging. *Neuroimage* 1996;4:34–54.
20. Songrass JG, Vanderwart M. A standardized set of 260 pictures: norms for name agreement, image agreement, familiarity, and visual complexity. *J Exp Psychol[Hum Learn Mem]* 1980;6:174–215.
21. DeGrado TR, Turkington TG, Williams JJ, Stearns CW, Hoffman JM. Performance characteristics of a whole-body PET scanner. *J Nucl Med* 1994;35:1398–406.
22. Lewellen TK, Kohlmeyer SG, Miyaoka RS, Kaplan MS. Investigation of the performance of the General Electric Advance positron emission tomograph in 3D mode. *IEEE Trans Nucl Sci* 1996;43:2199–206.
23. Sadato N, Carson RE, Daube-Witherspoon ME, Campbell G, Hallett M, Herscovitch P. Optimization of noninvasive activation studies with ^{15}O-water and three-dimensional positron emission tomography. *J Cereb Blood Flow Metab* 1997;17:732–9.
24. Kinahan PE, Rogers JG. Analytic three dimensional image reconstruction using all detected events. *IEEE Trans Nucl Sci* 1989;36:964–8.
25. Bandettini PA, Jesmanowicz A, Wong EC, Hyde JS. Processing strategies for time-course data sets in functional MRI of the human brain. *Magn Res Med* 1993;30:161–73.
26. Talairach J, Tournoux P. *Co-planar stereotaxic atlas of the human brain.* New York: Thieme, 1988.
27. Petersen SE, Fox PT, Posner MI, Mintun M, Raichle ME. Positron emission tomographic studies of the cortical anatomy of single-word processing. *Nature* 1988;331:585–9.
28. Grabowski TJ, Frank RJ, Brown CK, et al. Reliability of PET activation across statistical methods, subject groups, and sample sizes. *Hum Brain Map* 1996;4:23–46.
29. Wise R, Chollet F, Hadar U, Friston K, Hoffner E, Frackowiak R. Distribution of cortical neural networks involved in word comprehension and word retrieval. *Brain* 1991;114:1803–17.
30. Raichle ME, Fiez JA, Videen TO, et al. Practice-related changes in human brain functional anatomy during nonmotor learning. *Cereb Cortex* 1994;4:8–26.
31. Haxby J, Horwitz B, Ungerleider L, Maisog J, Pietrini P, Grady C. The functional organization of human extrastriate cortex: a PET-rCBF study of selective attention to faces and locations. *J Neurosci* 1994;14:6336–53.
32. Kawashima R, O'Sullivan BT, Roland PE. Positron-emission tomography studies of cross-modality inhibition in selective attentional tasks: closing the "mind's eye." *Proc Natl Acad Sci USA* 1995;92:5969–72.
33. Born P, Rostrup E, Leth H, Peitersen B, Lou HC. Change of visually induced cortical activation patterns during development. *Lancet* 1996;347:543.
34. Frahm J, Merboldt KD, Hanicke W. Direct FLASH imaging of magnetic field inhomogeneities by gradient compensation. *Magn Res Med* 1988;6:474–80.
35. Ordidge RJ, Gorell JM, Deniau JC, Knight RA, Helpern JA. Assessment of relative brain iron concentrations using T2-weighted and T2*-weighted MRI at 3 Tesla. *Magn Res Med* 1994;32:335–41.
36. Yang QX, Dardzinski BJ, Li S, Eslinger PJ, Smith MB. Multi-gradient echo with susceptibility inhomogeneity compensation (MGESIC): demonstration of fMRI in the olfactory cortex at 3.0 T. *Magn Res Med* 1997;37:331–5.